International Journal of Plasticity 47 (2013) 126–142

Contents lists available at SciVerse ScienceDirect

International Journal of Plasticity

journal homepage: www.elsevier.com/locate/ijplas

Dislocation motion in tungsten: Atomistic input to discrete dislocation simulations

K. Srivastava [a,*], R. Gröger [b], D. Weygand [a], P. Gumbsch [a,c]

[a] Institute for Applied Materials IAM, Karlsruhe Institute of Technology, 76131 Karlsruhe, Germany
[b] Central European Institute of Technology–Institute of Physics of Materials (CEITEC–IPM), Academy of Sciences of the Czech Republic, Žižkova 22, 616 62 Brno, Czech Republic
[c] Fraunhofer-Institut für Werkstoffmechanik IWM, Wöhlerstr. 11, 79108 Freiburg, Germany

ARTICLE INFO

Article history:
Received 18 September 2012
Received in final revised form 9 January 2013
Available online 4 February 2013

Keywords:
Body-centered cubic
Non-Schmid effects
Anomalous slip
Discrete dislocation dynamics

ABSTRACT

A computational framework for the discrete dislocation dynamics simulation of body-centered cubic (*bcc*) metals which incorporates atomistic simulation results is developed here on the example of tungsten. Mobility rules for the a/2⟨111⟩ screw dislocations are based on the kink-pair mechanism. The fundamental physical quantity controlling the kink-pair nucleation, the stress-dependent activation enthalpy, is obtained by fitting the line-tension model to atomistic data extending the approach by Gröger et al. (2008a,b) and Gröger and Vitek (2008c). In agreement with atomistic simulation, kink-pair nucleation is assumed to occur only on {110} planes. It is demonstrated that slip of the crystal along high-index planes like {112} which is often observed in experiments is obtained by the glide of the dislocation on two or more {110} planes. It is shown that such an atomistic based description of the dislocation mobility provides a physical basis to naturally explain many experimentally observed phenomena in *bcc* metals like the tension–compression asymmetry, the orientation dependence of loading, temperature dependence of yield stress and the crystallography of slip.

1. Introduction

Since the early studies of plastic flow in α-iron by Taylor and Elam (1926), it has been known that slip in body-centered cubic (*bcc*) metals occurs by sliding along crystallographic planes parallel to the ⟨111⟩ direction. Their early observations, combined with later experimental evidence confirmed that yielding in *bcc* metals does not obey the well-known Schmid law (Schmid and Boas, 1935) used to describe the plastic flow of face-centered cubic (*fcc*) metals. An implication of this law is that there exists a well defined critical resolved shear stress (CRSS) to initiate plastic flow that is independent of the orientation of applied loading and the sense of shearing on a crystallographic plane and that is not affected by components of the stress tensor other than the resolved shear stress (Duesbery, 1986). Accordingly, plastic flow is expected to initiate on the plane having the highest resolved shear stress. However, many experiments on various *bcc* metals (Christian, 1983) have revealed that these metals display features like the temperature and strain-rate dependence of yield and flow stresses. Fracture experiments on tungsten single crystals (Riedle et al., 1996; Gumbsch et al., 1998; Gumbsch, 2003) also show that the fracture toughness and the brittle to ductile transition are both directly correlated with the temperature and strain rate dependent changes of dislocation mobility (Hartmaier and Gumbsch, 2005). Single crystal deformation experiments in *bcc* metals (Christian, 1983) generally show a tension–compression asymmetry, and/or a twinning-antitwinning

* Corresponding author.
E-mail address: kinshuk.srivastava@kit.edu (K. Srivastava).

0749-6419/$ - see front matter © 2013 Elsevier Ltd. All rights reserved.
http://dx.doi.org/10.1016/j.ijplas.2013.01.014

asymmetry which all clearly contradict the Schmid law and are, therefore, referred to as non-Schmid behavior. Low-temperature experiments in tension and compression on high-purity single crystals of niobium (Duesbery and Foxall, 1969; Bolton and Taylor, 1972) and molybdenum (Jeffcoat et al., 1976; Matsui et al., 1976) have further shown that for some orientations, the plastic flow occurs on planes that are not the most highly stressed. This phenomenon is known as anomalous slip.

The non-planar spreading of the dislocation core of screw dislocations in *bcc* metals, first proposed by Hirsch (1960), provides an explanation for the large Peierls stresses in these materials and the orientation dependence of the CRSS. The importance of dislocation core structure and dislocation core effects on the mechanical properties of different metals has been emphasized in the review by Vitek (1992). Most importantly core effects lead to a temperature dependence of the flow stress due to the overcoming of the intrinsic energy barriers, the Peierls barriers, by the kink-pair nucleation mechanism (Seeger, 1956; Dorn and Rajnak, 1964).

Atomistic investigations of an isolated a/2⟨111⟩ screw dislocation in molybdenum and tungsten (Ito and Vitek, 2001) revealed that the dislocation core and hence the Peierls barrier is strongly affected by the shear stresses parallel to the slip direction acting in a different plane of the corresponding ⟨111⟩ zone than the slip plane, and the shear stresses perpendicular to the slip direction. These components are non-glide stresses. The latter do not exert any direct glide force on the dislocation but break the symmetry of the dislocation core and thus promote slip on the {110} plane into which the dislocation core is predominantly extended (Gröger et al., 2008a). It is important to note that other stress components than these two shear stresses do not play any major role (Ito and Vitek, 2001).

Recently, Gröger et al. (2008a) and Gröger and Vitek (2005) utilized Bond Order Potentials (BOP) for molybdenum and tungsten (Mrovec et al., 2004; Mrovec et al., 2007) to calculate the dependence of the Peierls stress on the orientation of the maximum resolved shear stress plane (MRSSP) in uniaxial loading and on the magnitude of the shear stress perpendicular to the slip direction. They found a strong twinning-antitwinning asymmetry in molybdenum but virtually none in tungsten. Additionally, the most active slip system did not systematically coincide with the most highly stressed {110}⟨111⟩ glide system but varied with both the orientation of the MRSSP and the magnitude of the shear stress perpendicular to the slip direction. Based on these results, they developed a two-dimensional Peierls potential that changes its shape in response to the non-glide stress components and orientation of the MRSSP (Gröger and Vitek, 2008c). This was utilized to develop a thermodynamic model of the dislocation glide at finite temperatures, which is based on the classical works of Seeger (1956) and Dorn and Rajnak (1964). It was thus possible to obtain physically justified flow criteria for molybdenum and tungsten that originate at the level of isolated a/2⟨111⟩ screw dislocations. By scaling the atomistically obtained stresses by a factor of roughly 3–4, this multiscale approach was shown to yield reasonable macroscopic predictions of cavitation instability and the occurrence of strain bursts in bcc metals (Gröger and Vitek, 2008c; Racherla and Bassani, 2007). However, no attempt has been made to directly employ the atomistic simulation results to study the general dislocation–dislocation interactions in these materials.

Discrete dislocation dynamics (DDD) models can provide the link between single dislocation properties, dislocation microstructure and multi-dislocation interactions, and the macroscopic response. This of course requires a physically based modeling of the mobility of screw dislocations in *bcc* metals. Screw dislocation mobility is determined from the activation enthalpy of kink-pair nucleation. Current modeling approaches in DDD are based on parametrizing the activation enthalpy of kink-pair nucleation on screw dislocations using the phenomenologically based Kocks model whose parameters are fitted to experiments (Tang et al., 1998; Naamane et al., 2010). This description remains macroscopic in nature as the activation enthalpy is a function of effective global resolved shear stress. Such a model therefore does not account for the core effects on screw dislocation mobility and is not predictive in nature. More recently Chaussidon et al. (2008) have partially incorporated non-Schmid behavior via cross-slip rules in DD simulations based on atomistic information. These rules give rise to an asymmetric glide in tension and compression loadings. Wang and Beyerlein (2011) utilize atomistic information to incorporate the effects of the non-glide components of the stress-tensor on screw dislocation mobility within the Kocks model framework.

A straightforward implementation of the atomistic information into DDD is also not feasible since the atomistic modeling has its limitations in the accessible length and time scales. Mesoscopic models such as DDD have to handle longer length and time scales, which necessitates a systematic information transfer from the atomistic scale to dislocation properties in the form of a constitutive law for the dislocation mobility, which at the same time, retains the fundamental physics.

In this article, we present an approach to transfer the results of atomistic studies to a mesoscopic DDD model which takes into account the screw dislocation core effects on dislocation mobility at the scale of DDD. The motion of each screw dislocation in DDD is governed by the local stress state along the dislocation. We start with an isolated screw dislocation and will discuss the response of this particular dislocation under different loading conditions in detail within the non-Schmid framework at various temperatures.

The approach we present here is different from a continuum description of plastic flow like that presented in Gröger et al. (2008b) and Gröger and Vitek (2008c). In such a continuum formulation the glide system, which is most easily activated, defines the inner envelope of the yield surface. In DDD simulations, the response of any given dislocation to the local stress state has to be followed. This requires a somewhat more general approach. In agreement with atomistic studies, the elementary slip planes of screw dislocations are taken as {110} planes only. The most important experimentally observed phenomena like the tension–compression asymmetry at finite temperatures (Christian, 1983) and even changes of effective slip planes with temperature will be shown to be a natural consequence of this modeling and of the incorporation of the

non-Schmid stress components. The temperature dependence of the critical stress required to activate a screw dislocation based on kink-pair nucleation theory is simulated for different orientations under uniaxial tension and compression.

2. Modeling aspects

A physically based model of the a/2⟨111⟩ screw dislocation mobility suitable for use within a DDD framework (Weygand et al., 2008, 2002; Weygand and Gumbsch, 2005) is presented in this section. The parameters of the mobility law are based on the atomistic approach of Gröger et al. (2008a,b) and Gröger and Vitek (2008c), which was extended in order to include all possible glide planes for each screw dislocation as described later. Within the DDD framework, the local stresses acting on the screw dislocation are known and therefore a local mobility law is formulated. To connect both, the atomistic and discrete dislocation framework, the parametrization used for the atomistic results is presented in Section 2.2. Since the non-planar screw dislocation core structure is not explicitly modeled at the DDD scale, the asymmetry induced in the core structure due to applied loading must be accounted for appropriately in the mesoscopic mobility rule in order to capture the true mechanisms of dislocation activation and motion.

2.1. Modeling of non-screw dislocations

In our model, all non-screw segments move by the phonon-drag mechanism parametrized by a kinetic law that takes into account inertial effects (Weygand and Gumbsch, 2005; Bitzek and Gumbsch, 2005).

$$m_0 \frac{\partial v}{\partial t} + Bv = \tau_{glide} b \tag{1}$$

$$\tau_{glide} = \mathbf{b} \cdot \overline{\boldsymbol{\sigma}}_{tot} \cdot \mathbf{n} \tag{2}$$

where m_0 is the mass per unit length of dislocation, v the dislocation velocity and $\mathbf{b}$ and $\mathbf{n}$ the Burgers vector and glide plane normal respectively. B is material specific temperature-dependent drag-coefficient that could in principle be obtained from molecular dynamics (MD) studies (see e.g. Bitzek and Gumbsch, 2005). For non-screw dislocations, B is simply taken as a constant ($B = 10^{-4}$ Pa s). The glide component of the Peach-Koehler force $\tau_{glide} b$ on a dislocation is obtained from the local stress state using Eq. (2). The total local stress $\overline{\boldsymbol{\sigma}}_{tot}$ is the sum of the external applied stress, image stresses and the stress due to all dislocations and the boundary conditions of the elastic problem.

2.2. Atomistics of single screw dislocations and parametrization of loading

Here we introduce some basic definitions used throughout this article in a similar manner as in the literature (Gröger et al., 2008a; Christian, 1983). These definitions are applicable to any loading axis within the [001] – [011] – [$\bar{1}$11] stereographic triangle which is shown in Fig. 1. For macroscopic uniaxial loading, all possible loading axes in a *bcc* crystal can be found in this stereographic triangle.

1. *MRSSP*: The maximum resolved shear stress plane as shown in Fig. 2 whose orientation is defined as the angle χ it makes with the ($\bar{1}$01) plane. For reasons of crystal symmetry, it is sufficient to consider the range $-30^\circ \leqslant \chi \leqslant 30^\circ$.
2. The *twinning* ($\chi < 0$) and *antitwinning* ($\chi > 0$) sense of shearing on the nearest {112} plane (Fig. 2).
3. *CRSS*: The critical resolved shear stress acting on the *MRSSP* which indicates the shear (glide) stress required to move the dislocation in any of the {110} planes.
4. The angle $\bar{\psi}$ between the ($\bar{1}$01) plane and the observed macroscopic slip plane.

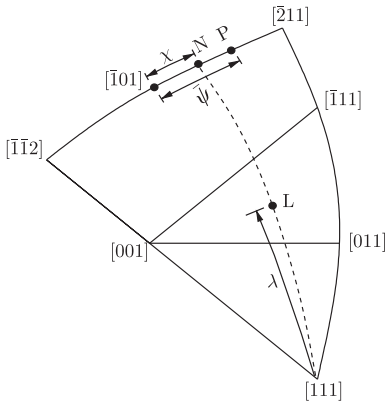

Fig. 1. Loading axes in the [001] – [011] – [$\bar{1}$11] stereographic triangle. The point L represents the orientation of the loading axis, P the direction normal to the slip plane and N is direction normal to the MRSSP.

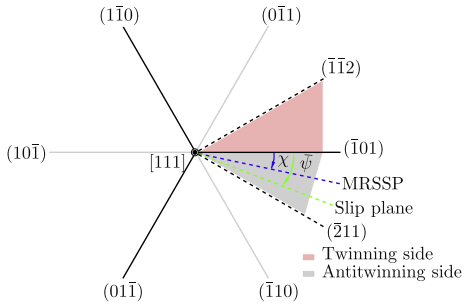

Fig. 2. Orientations of planes in the [111] zone.

The three {110} planes that contain a given Burgers vector are called the zonal planes. The stress tensor that affects the magnitude of the *CRSS* to move a screw dislocation on either of the planes in the zone of the given Burgers vector is given by Gröger et al. (2008a,b)

$$\overline{\boldsymbol{\Sigma}}^{\chi} = \begin{bmatrix} -\sigma & 0 & 0 \\ 0 & \sigma & \tau \\ 0 & \tau & 0 \end{bmatrix} \tag{3}$$

This tensor is obtained by transforming the stress tensor of applied loading into a right-handed system defined by the z-axis parallel to the Burgers vector, the y-axis normal to the MRSSP and the x-axis in the MRSSP. The shear stress perpendicular to the slip direction σ, and the shear stress parallel to the slip direction τ are the only non-zero components of the local stress tensor $\overline{\boldsymbol{\Sigma}}^{\chi}$. The notation here for shear stress parallel and perpendicular to Burgers vector has been interchanged compared to Gröger et al. (2008b). This has been done to make it consistent with conventional literature (Brunner and Glebovsky, 2000; Hull and Bacon, 2001; Hirth and Lothe, 1982). It was shown in Ito and Vitek (2001) that the other components of the stress tensor $\overline{\boldsymbol{\Sigma}}^{\chi}$ have no effect on the CRSS. This suggests that the CRSS-σ relationship is unique for a given χ and is independent of the loading history (Gröger et al., 2008b).

There are 12 crystallographically equivalent $\{110\}\langle 111\rangle$ slip systems in *bcc* crystals. Slip on higher index planes is assumed to be composed of steps on the elementary {110} planes. In order to differentiate between the twinning and antitwinning sense of shearing, positive and negative slip directions are treated as being distinct. This results in 24 distinct $\{110\}\langle 111\rangle$ slip systems.

2.3. Screw dislocation mobility

It is generally accepted that screw dislocations in *bcc* metals overcome the Peierls barrier by thermally activated and stress-assisted generation of kink pairs (Dorn and Rajnak, 1964; Guyot and Dorn, 1967). According to the transition state theory, the average forward velocity of screw dislocations is given as (Dorn and Rajnak, 1964; Guyot and Dorn, 1967)

$$v = \frac{ba_0 L}{l_c^2} v_D \exp\left(\frac{-\Delta H(\overline{\boldsymbol{\Sigma}}^{\chi})}{k_B T}\right) \tag{4}$$

where v_D is the Debye frequency, b the magnitude of the Burgers vector, a_0 the height of the kink ($a_0 = a\sqrt{2/3}$), a the lattice constant, L the length of the screw dislocation, l_c the critical length for the nucleation of a kink pair, k_B the Boltzmann factor, T the absolute temperature and $\Delta H(\overline{\boldsymbol{\Sigma}}^{\chi})$ the stress-dependent activation enthalpy. Note that ΔH is written as a function of $(\overline{\boldsymbol{\Sigma}}^{\chi})$ from Eq. (3) to indicate its dependence on the entire stress tensor and not as a function of the resolved shear stress τ alone. The term L/l_c gives the number of possible nucleation sites for kink pairs implying that the rate of kink nucleation is dependent on the length L of the screw dislocation. Because of the exponential dependence in Eq. (4) the dominating term in the velocity relation is the stress-dependent activation enthalpy and hence its determination plays a crucial role in describing the kinetics of screw dislocations.

2.3.1. Enthalpy of kink pair nucleation

The atomistic and mesoscale models can be linked by the stress dependent activation enthalpy $\Delta H(\overline{\boldsymbol{\Sigma}}^{\chi})$ for kink pair nucleation. The activation enthalpy is a measure of the remaining energy needed by the embryonic kinks to reach the saddle point configuration after accounting for the mechanical part of the loading due to glide stress. Just like the CRSS, the kink pair activation enthalpy must also be a function of the non-Schmid components σ, the angle of the MRSSP χ and the glide stress τ. Instead of explicitly accounting for σ, it is preferable to consider the ratio $\eta = \sigma/\tau$. Hence the activation enthalpy can be mathematically represented as $\Delta H(\chi, \eta, \tau)$. Theoretically, the activation enthalpy can be described by two different analytical models depending on the temperature regime. These are the line-tension (LT) (Dorn and Rajnak, 1964) model for the

low-temperature and high stress regime and the elastic-interaction model (EI) (Seeger, 1956; Caillard and Martin, 2003) for the high temperature and low stress regime. These models differ in the saddle-point configuration for the nucleation of a kink pair out of a straight screw dislocation. The LT-model has been used here to obtain the activation enthalpies from the atomistic data (Gröger and Vitek, 2008c).

At finite applied stresses the dislocation is moved away from the bottom of the Peierls valley by the action of the shear stress τ. The path of the dislocation line is curvilinear and the distance of the dislocation along this curve is denoted by ξ. The position along this path at which the force $dV/d\xi$, originating from the Peierls potential, is equal to the glide component of the total Peach-Koehler force τb, is denoted by ξ_0. Following Dorn and Rajnak (1964), the activated state is then represented by a continuous bow-out of a finite segment of the initially straight dislocation from ξ_0 to the position ξ_c which represents the critical state. This activated state is defined as the difference between the line energy of the dislocation, represented by the height of the Peierls potential, and the work done by the applied stress on overcoming the Peierls barrier. This yields the relation $V(\xi_c) - V(\xi_0) = \tau b(\xi_c - \xi_0)$ that allows one to calculate ξ_c if the Peierls barrier $V(\xi)$ is known. Hence, the activation enthalpy takes the form (Dorn and Rajnak, 1964)

$$\Delta H(\chi, \eta, \tau) = 2\int_{\xi_0}^{\xi_c} \sqrt{[V(\xi)]^2 - [\tau b(\xi - \xi_0) + V(\xi_0)]^2}\,\mathrm{d}\xi \tag{5}$$

The calculation of the activation enthalpy at finite applied stresses from Eq. (5) requires explicit knowledge of the Peierls barrier $V(\xi)$ and its intrinsic dependence on χ, σ and τ. The calculation of the Peierls barrier has been a major theoretical problem. Recently two methods were proposed to calculate the Peierls barrier using the Nudged Elastic band method (NEB). One is based on the calculation of the activation enthalpy of the dislocation with a continuous bow-out in the direction of the applied load (Rodney and Proville, 2008). The other provides directly the Peierls barrier for a straight screw dislocation using a modified version of the NEB method that includes atomic relaxations (Gröger and Vitek, 2012).

The construction of the Peierls potential for tungsten and the calculation of the stress dependence of the activation enthalpy is taken from atomistic data (Gröger et al., 2008a,b,c) for isolated screw dislocations. The corresponding details of the construction of the Peierls barrier is discussed in these references.

2.3.2. Kinetics of screw dislocations

The glide of the a/2⟨111⟩ screw dislocation is possible in any of the three crystallographic planes of {110} type in the zone of this direction, namely, $(\bar{1}01)$, $(0\bar{1}1)$ and the $(\bar{1}10)$ planes as shown in Fig. 3. Kink-pair nucleation is in principle possible on each of these three crystallographic planes parametrized with $\psi = 0°,\ -60°,\ +60°$, respectively. The dislocation motion on any of the three planes in the zone of the Burgers vector is possible and the corresponding kink pair nucleation enthalpy is obtained from Eq. (5).

Our modeling is based on the simple idea that the dislocation will have the highest kink-pair nucleation probability on the plane with the lowest activation enthalpy for a given loading state. In the absence of applied stress, the Peierls barrier is the same on each of these {110} planes in the zone of the Burgers vector and therefore, the transition probability of the dislocation from lattice site L_0 to the next Peierls valley (L_1, L_2 or L_3) in Fig. 3 is the same due to symmetry. Under any loading, the transition probability is different for the three planes due to the work term $\tau b(\xi - \xi_0)$ in Eq. (5). Additionally,

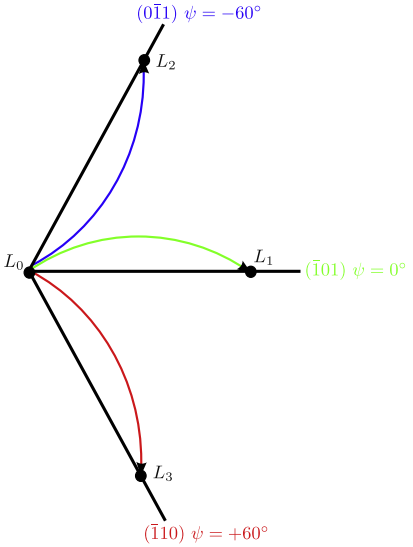

Fig. 3. Schematic paths of the screw dislocation for slip on the three {110} zonal planes.

as can be concluded from the atomistic simulations (Gröger et al., 2008a,b,c), the Peierls barrier $V(\xi)$ on each of the corresponding zonal planes of the screw dislocation is deformed. This changes the activation enthalpy and the Peierls stress on the corresponding plane. In the absence of thermal activation, the dislocation would move on the plane where the resolved stress first reaches the Peierls stress. At finite temperature, the activation enthalpy is the determining factor for kink-pair nucleation and Eq. (4) gives an average forward magnitude of velocity v_ψ on each of the possible transition $\{110\}$ planes

$$v_\psi = \frac{ba_0L}{l_c^2} v_D \exp\left(\frac{-\Delta H_\psi}{k_B T}\right) \tag{6}$$

This directly leads to the highest velocity on the plane with the lowest ΔH_ψ. Hence the problem effectively reduces to determining the dependence of the kink pair nucleation enthalpies ΔH_ψ on χ, η and τ for the planes $\psi = 0^\circ, -60^\circ$ and $+60^\circ$. This has been done for tungsten extending thus the results presented in Gröger et al. (2008b) which consider the plane $\psi = 0^\circ$ only.

In the DDD-model, the activation enthalpy that will be used in our simulations is supplied as a lookup table $(\chi, \eta, \tau) \rightarrow \Delta H_\psi$ from atomistics calculations for a number of discrete orientations of the MRSSP (angle χ) and some discrete values of ratios of the two shear stresses, η. A plot for a specific parameter set is shown in Fig. 4. Since the dislocation can move by elementary steps on the three $\{110\}$ planes, three tables are provided that give the activation enthalpies $\Delta H_\psi(\psi = 0^\circ, -60^\circ, +60^\circ)$. To calculate $\Delta H_\psi(\chi, \eta, \tau)$ for a given direction corresponding to any arbitrary stress state, a trilinear interpolation scheme is used.

Once the activation enthalpy ΔH_ψ on each of these three $\{110\}$ planes is calculated, the total forward velocity of the screw dislocation resulting from motion on elementary slip planes is written as

$$\mathbf{v}_{gl} = \sum_\psi v_\psi \mathbf{e}_\psi, \quad \text{where } \psi = -60^\circ, 0^\circ, +60^\circ \tag{7}$$

Here, $\mathbf{e}_\psi$ is the corresponding unit vector in the translation direction and v_ψ the corresponding magnitude. The angle $\overline{\psi}$ between the effective slip plane and the $(\bar{1}01)$ plane can be computed from the velocity vector using

$$\overline{\psi} = -\sin^{-1} \frac{\mathbf{v}_{gl} \cdot \mathbf{n}}{|\mathbf{v}_{gl}|} \tag{8}$$

where $\mathbf{n}$ is the unit normal to the $(\bar{1}01)$ or $(10\bar{1})$ plane. The effectiveness of this approach will be demonstrated in the examples that follow in Section 3. Due to the exponential dependence of the velocity on ΔH_ψ, the glide velocity in Eq. (7) is dominated by the v_ψ for that particular $\{110\}$ plane for which ΔH_ψ is lowest.

Eq. (7) implicitly assumes that the stress state does not vary along the screw dislocation. This is not true in general, as local stresses within the sample depend on both other dislocations and stress gradients due to chosen boundary conditions. Even though the screw dislocation shown in Fig. 5 is initially a straight line of length L, its geometrical representation within the DDD framework is done by a sequence of n aligned segments of length l_i ($L = \sum_{i=1}^{n} l_i$), following the concept of the DDD model described in Weygand et al. (2002). The lengths of the segments l_i are adapted to the local dislocation density and the minimal distance to the closest dislocation to capture local stress variations along the dislocation line. A further restriction on the length l_i of each dislocation segment applies: it is always greater than the critical length l_c required for kink nucleation. The kinks on dislocations are generally of the order of one to a few lattice spacings, a length scale which shall not

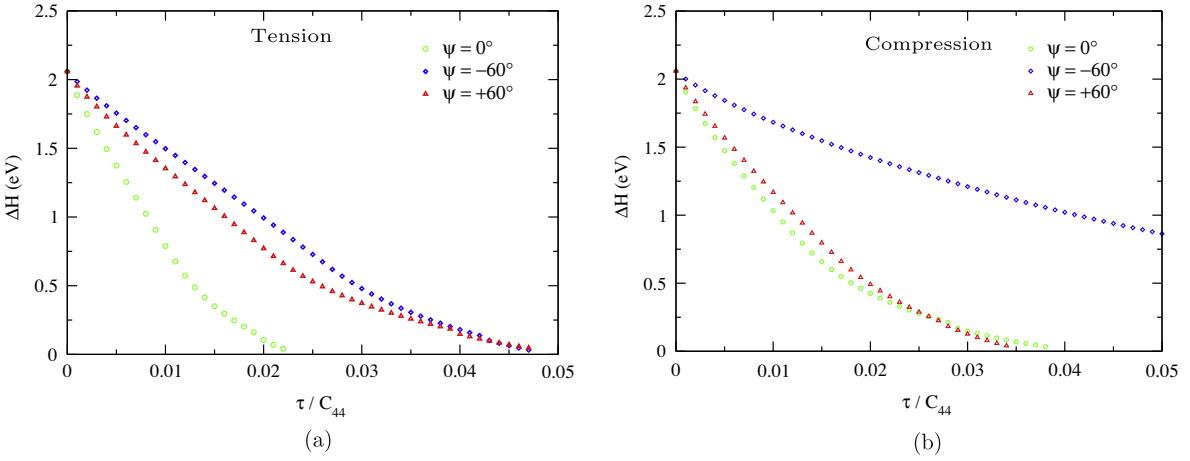

Fig. 4. Example of plot of $\Delta H_\psi(\chi = 10^\circ, \eta = \pm 0.5)$ vs τ: (a) corresponds to $\eta = +0.5$, while (b) is for $\eta = -0.5$.

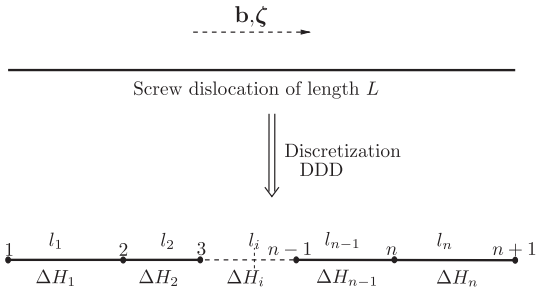

Fig. 5. Velocity computation scheme within DDD framework for a screw dislocation of total length L with Burgers vector and line direction **b** and ζ, respectively. The dislocation is discretized into n segments, each of length l_i, in order to evaluate the local activation enthalpy ΔH_i.

be resolved at the mesoscopic scale of DDD simulations. The kinks on screw dislocations generated after cross-slip have length of $5a_0$. To simplify the following arguments, we assume for the moment that the entire screw dislocation remains on the same glide plane. The average forward velocity of each segment i of length l_i is then given by

$$v_i = \frac{ba_0 l_i}{l_c^2} v_D \exp\left(\frac{-\Delta H_i}{k_B T}\right) \tag{9}$$

From this equation the local kink-pair production rate of each segment i is known. We assume that the time of migration of a kink t_{mig} along the entire screw dislocation of length L is short compared to the time between two nucleation events t_{nuc}. This assumption is certainly valid in the low and medium temperature range (Seeger, 2002). Thus every successful kink generation on each segment i contributes to the forward motion of the entire screw dislocation. Hence the velocities of all the individual segments of a dislocation line are added. The entire dislocation of length L moves forward with the total velocity

$$V_L = \sum_{i=1}^{n} v_i \tag{10}$$

The consistency of this approach is easily demonstrated assuming a homogeneous stress state along the entire dislocation of length L, numerically represented by n segments of lengths l_i, which results in equal activation energies for all segments $\Delta H_i = \Delta H$. From Eq. (10), the average velocity of the screw dislocation results in the expected velocity from Eq. (4):

$$V_L = \underbrace{(l_1 + l_2 + \cdots l_n)}_{L} \frac{ba_0}{l_c^2} v_D \exp\left(\frac{-\Delta H}{k_B T}\right) \tag{11}$$

The direction of motion of the dislocation is given by Eq. (7).

The simplification that the entire screw dislocation remains on the same plane, is easily overcome. To do so, one has to identify after evaluation of the local stresses those sections of the screw dislocation, which will glide on the same plane. This allows the initially straight screw dislocation to change glide plane and will automatically lead to the occurence of cross-slip and subsequently formation of cross-kinks.

3. Results

We will first consider the response of a non-interacting a/2[111] screw dislocation in tungsten under uniaxial tension and compression applied in different orientations, as shown in Fig. 6. For all the orientations considered, the $(\bar{1}01)$ crystallographic plane is the plane with the highest resolved shear stress parallel to the slip direction among the $\{110\}$ planes. The velocity of the screw dislocation is computed from Eq. (4).

In order to establish a yield criterion for single dislocations, an equivalent critical velocity is derived from the macroscopic strain rate given by the Orowan equation

$$\dot{\gamma} = \rho_m b v \tag{12}$$

where $\dot{\gamma}$ is the plastic shear strain rate, ρ_m the density of mobile screw dislocations, b the magnitude of Burgers vector and v the average velocity of the screw dislocation. For our computation, the chosen numerical values are $\rho_m = 10^{12}\ \mathrm{m}^{-2}$, $b = 2.741$ Å. The yield stress is defined to be the shear stress on the MRSSP required for the screw dislocation to attain a magnitude of velocity of 1 $\mu\mathrm{m\,s}^{-1}$ which corresponds to a plastic strain rate $\dot{\gamma} = 2.7 \times 10^{-4}\ \mathrm{s}^{-1}$ similar to the experiments on tungsten in Brunner (2004, 2010). The calculations were performed up to a temperature of 800 K which is the experimentally observed athermal temperature for tungsten obtained from experiments (Schneider et al., 2009).

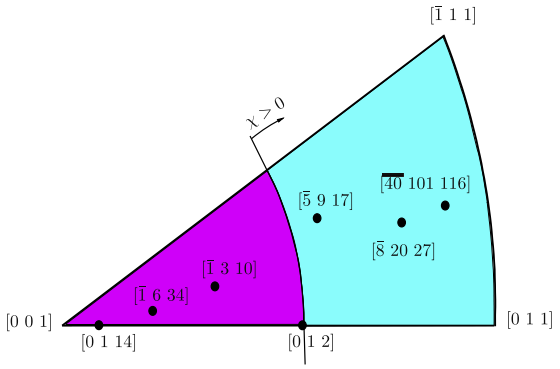

Fig. 6. Loading axes in [001] – [011] – [1̄11] stereographic triangle. The positive sense of χ means that the nearest {112} plane, i.e. $(\bar{2}11)$ is sheared in the antitwinning sense. The negative χ causes shearing of the nearest {112} plane, i.e. the $(1\bar{1}2)$ plane, in the twinning sense.

3.1. Tension–compression asymmetry and orientation dependence

Fig. 7 shows the CRSS as a function of temperature for three orientations depicted in Fig. 6. The general trend for all orientations is the same. The CRSS strongly decreases with increasing temperature, displaying two different regimes both in tension and compression. The high temperature, low stress regime is almost linear and dominated by the work term in Eq. (5), while all terms are important in the non-linear high stress regime. As an illustration, the two regimes are marked

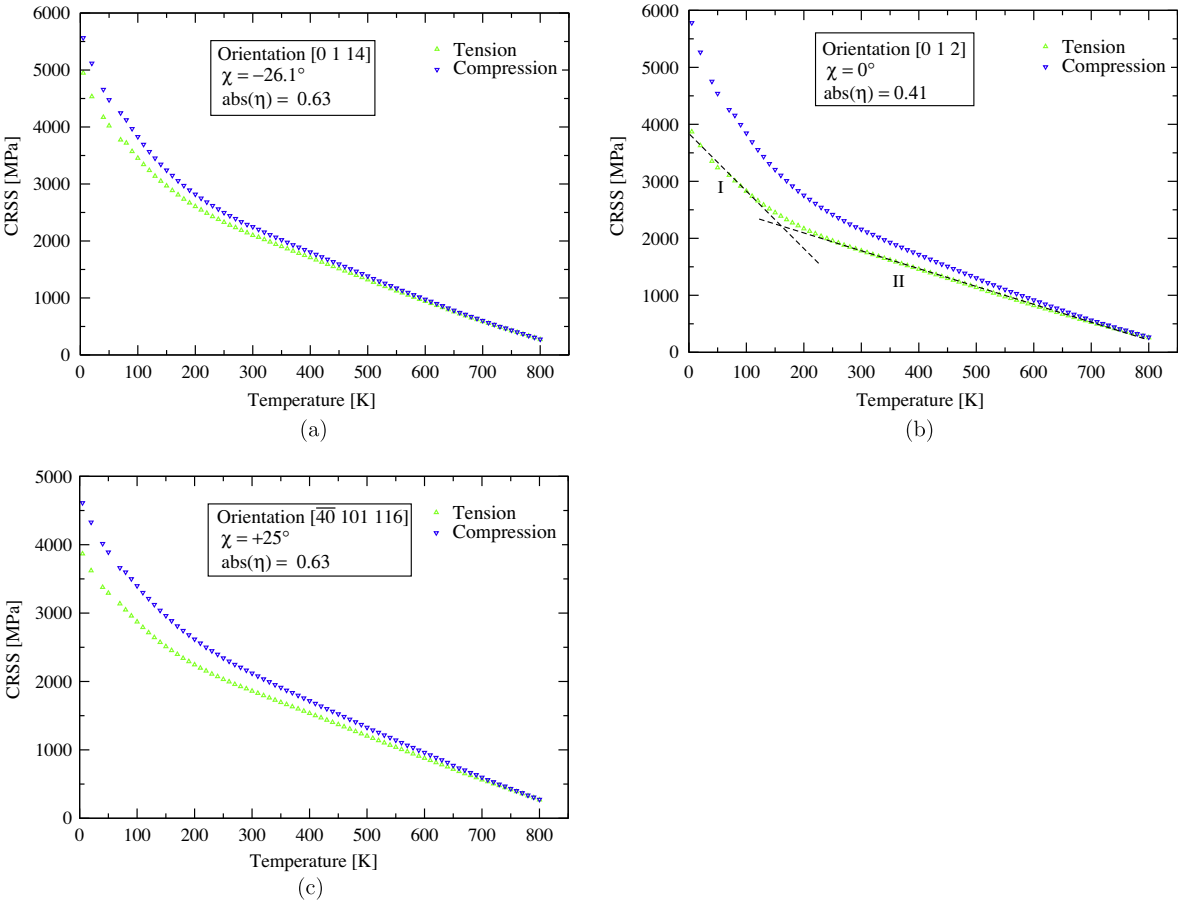

Fig. 7. CRSS vs temperature curves for different orientations of applied loading shown in the insets.

in Fig. 7(b) as II and I respectively. The CRSS depends on orientation and ranges from below 4 GPa to 6 GPa at 0 K. The orientation dependence of the CRSS is already much weaker at room temperature, where the values range from 1.8 to 2.3 GPa. The orientation dependence disappears at 800 K.

For the same orientation the sense of shearing is reversed and the shape of the CRSS-T-curve is somewhat different when changing from tension to compression. In terms of model parameters, each orientation corresponds to a different χ and η respectively. At lower temperatures, the CRSS in compression is always higher than in tension. The different orientations correspond to different non-Schmid stresses σ. In both tension and compression, the CRSS at 0 K obtained by extrapolation converge to different values and this value is additionally orientation dependent, in agreement with atomistic data at 0 K.

In tension, the glide plane is always the $(\bar{1}01)$ plane ($\overline{\psi} = 0^\circ$) for all orientations.

In compression, the atomistic data at 0 K (Gröger et al., 2008a,b) show that the dislocation always moves on the $(\bar{1}01)$ plane for orientations in the cyan region in Fig. 6, while the dislocation moves on the low-Schmid factor $(\bar{1}10)$ plane for orientations in the magenta region in Fig. 6. Hence the asymmetry in orientation dependence manifests itself not only in terms of the CRSS but also in terms of the preferred glide plane on which screw dislocations move. This atomistic aspect is recovered by our model and will be analyzed in more detail in Section 3.2.

3.2. Slip planes in tension and compression

Fig. 8 shows the variation of the macroscopic slip angle $\overline{\psi}$ with temperature T for different orientations in tension and compression obtained using Eq. (8).

In tensile loading and for temperatures up to 300 K, $\overline{\psi}$ stays at 0° which means that $|\mathbf{v}_{gl}|$ in Eq. (7) is determined entirely by the activation enthalpy on the $(\bar{1}01)$ plane irrespective of the orientation of the MRSSP and the magnitude of non-Schmid stresses. With increasing temperature $\overline{\psi}$ tends to deviate increasingly away from the $(\bar{1}01)$ plane and contributions from other {110} planes become significant. The average slip direction $\overline{\psi}$ moves towards the MRSSP. In tension, the slip angle $\overline{\psi}$ always stays within $\pm 30^\circ$ for all orientations in the entire temperature range. It is, however, interesting to note that the deviation of $\overline{\psi}$ from 0° towards χ occurs at lower temperatures for $\chi < 0$ as compared to $\chi > 0$.

For loading in tension and compression along the orientations for which $\chi < 0$ (magenta region in Fig. 6), the slip plane is $(\bar{1}01)$ ($\psi = 0^\circ$). For these orientations the temperature dependence of $\overline{\psi}$ in tension and compression is identical. For orientations with $\chi > 0^\circ$ (cyan region) the slip trace in compression is more complex. At low temperatures the glide plane is at $\overline{\psi} = +60^\circ$ ($(\bar{1}10)$ plane), while $\bar{\psi} = 0^\circ$ plane in tension. The slip trace at low temperature is well defined. Deviations from the $\psi = +60^\circ$ plane in compression, which may be viewed as an indication of wavy slip only occur at higher temperatures. With increasing temperature, the possibility of slip on the $\psi = 0^\circ$ plane becomes increasingly more significant and the average slip plane $\overline{\psi}$ also moves towards the MRSSP.

3.3. Frank–Read sources

Here we consider the activation of a single Frank–Read (FR) source shown in Fig. 9. The source is in edge orientation between the pinning points marked by **A** and **B** respectively and placed on the $(\bar{1}01)$ plane as shown. The length of the source is 380 nm. Such a source is subjected to both tension and compression loadings at the temperature of 200 K. The applied strain rate is 5000 s^{-1}. The source is placed in the middle of a pillar with edge length 1 μm and aspect ratio 1 : 2 : 1. Displacements along the loading direction are prescribed on the top and bottom surfaces. Rotational degrees of freedom (dof) are constrained and the remaining dofs have traction free boundary conditions.

The first activation of the source in tension geometrically follows the same steps as described in Tang et al. (1998) after the critical stress for bow-out of the source is reached on the $(\bar{1}01)$ plane. The non-screw oriented dislocation segments are highly mobile and escape the volume very quickly at low stresses, leaving two long screw dislocation dipoles. Thereafter each of the arms operates as an individual source. This is different from a FR-source in an *fcc* metal where the arms recombine resulting in a configuration involving the original FR-source surrounded by a dislocation loop.

The long screw dislocations move at atomistic values of the CRSS as shown in the stress strain curves in Fig. 11. A snapshot of operation of the source in tension and compression is shown for the orientation $[\bar{8}\,20\,27]$ in Figs. 9 and 10 respectively.

In tension (Fig. 9) the dislocation motion is confined to the most highly stressed $(\bar{1}01)$ plane. The mechanism of source operation is similar for all orientations and both the edge and screw dislocations move only on this plane. The formation of two arrays of screw dislocations with opposite line directions on either side of both pinning points is observed. The inner screw dislocations (3 and 4) between the pinning points annihilate.

In compression (Fig. 10), the source activation also begins with the motion of the edge dislocations on the highest resolved shear stress plane generating long screw dislocations on the $(\bar{1}01)$ plane. The screw segments then however move via cross-slip on the secondary plane $(\bar{1}10)$ which has the lowest activation enthalpy but not the highest resolved shear stress. Spiral sources are thereby generated on parallel planes which operate independently and no annihilation is therefore possible. This leads to an increase in dislocation density and a different internal stress state. The stress–strain curve for the single FR-source in tension and compression is shown in Fig. 11 with subscripts T and C respectively. The corresponding stress is then identified as the flow stress needed to maintain steady state plastic deformation in the pillar. The orientation dependence of flow stress in tension and compression can be identified. The flow stress in compression is always higher than

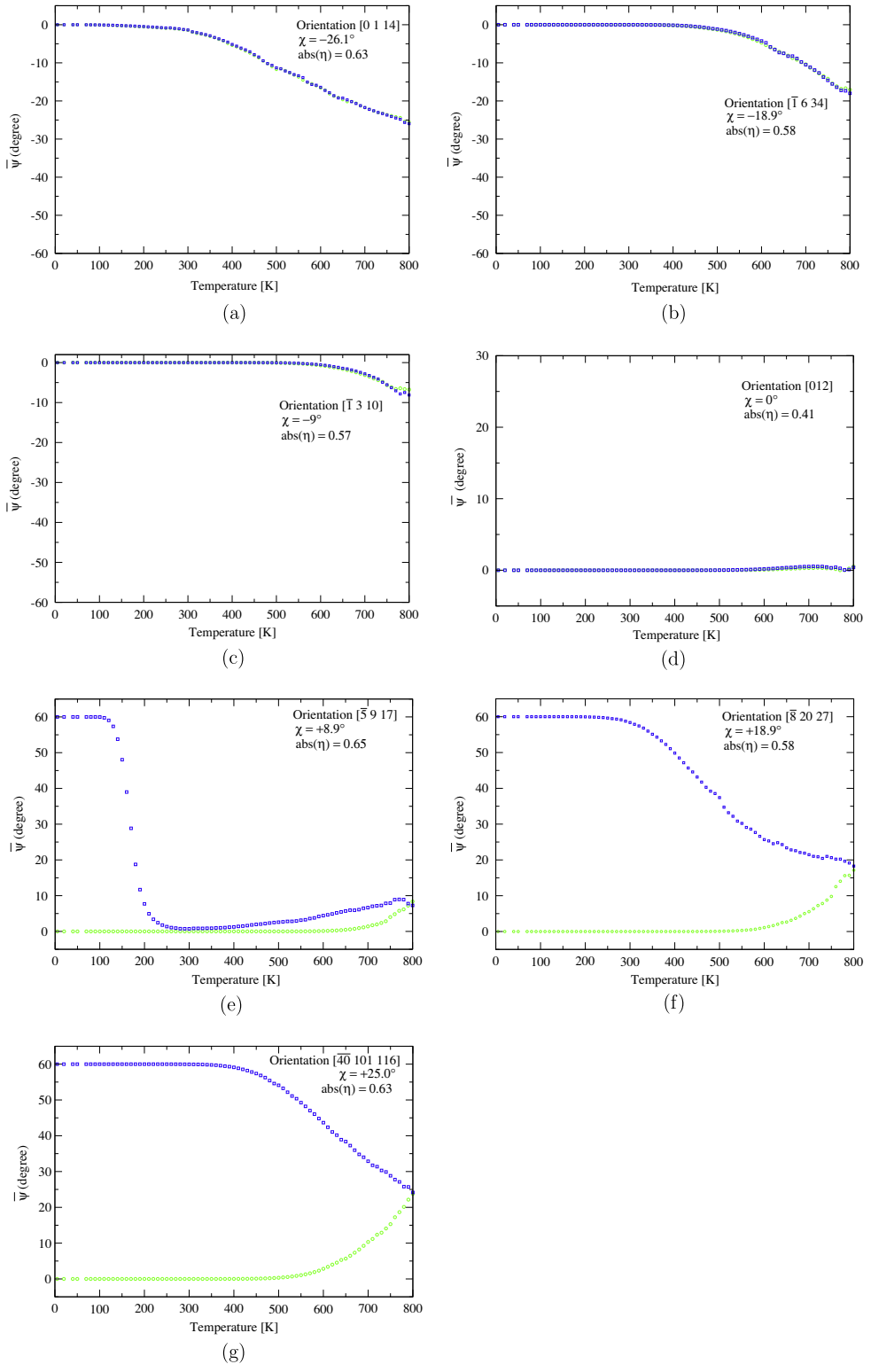

Fig. 8. Temperature dependence of $\bar{\psi}$ for different orientations: (○) for tension and (□) for compression.

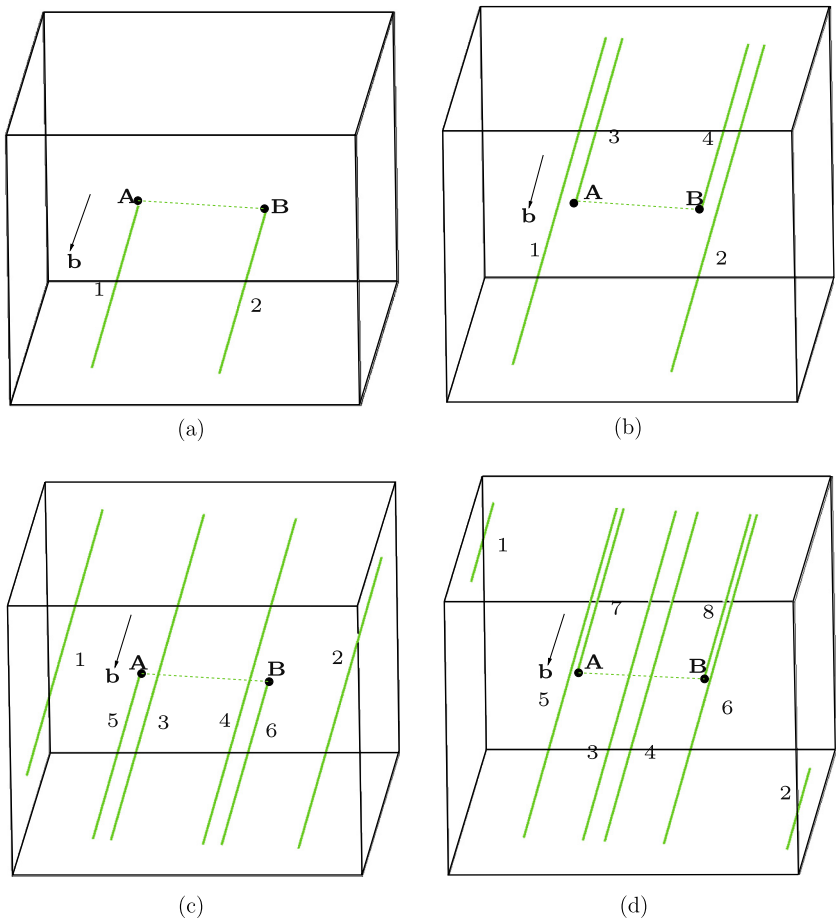

Fig. 9. The figures show successive steps of operation of the Frank–Read source with pinning points **A** and **B**, loaded in tension in the $[\bar{8}\ 20\ 27]$ direction. The dislocation lines are colored according to their habit plane. Green color of dislocation means it lies on the $(\bar{1}01)$ plane. In (a), the edge and mixed dislocations quickly move out of the volume leaving behind the screw dipoles formed by 1 and 2; (b) the screw dislocations get activated at their CRSS which generate small edge dislocations around the pinning points. These edge dislocations quickly leave the volume and generate further screw dislocation dipoles 3 and 4 respectively; (c) These newly generated spiral sources upon loading get activated upon further loading get activated and create the inner screw dipoles 3 and 4. The source now consists of dislocation arms 5 and 6; (d) dislocation 1 and 2 leave the volume and 3 and 4 annihilate each other as they are dipoles moving on the same plane. This sequence of steps is repeated with generation of dipoles around the pinning points. (For interpretation of the references in color in this figure legend, the reader is referred to the web version of this article.)

in tension. After yielding in both tension and compression, a constant flow-stress is required for the periodic activation of the single-armed sources.

4. Discussion

A mesoscopic model for the motion of screw dislocations in *bcc* metals suitable for application in DDD simulations and based directly on atomistic data (Gröger et al., 2008a,b,c) is presented here. The model is calibrated against the input atomistic data on single dislocations subjected to uniaxial loading in tension and compression. The CRSS required to activate a single screw dislocation is in agreement with the atomistic studies of isolated screw dislocations at 0 K.

4.1. Tension–compression asymmetry and orientation dependence

Over the years, experiments on *bcc* metals like tungsten (Argon and Maloof, 1966; Hull et al., 1967), molybdenum (Seeger and Hollang, 2000; Christian, 1983) and tantalum (Hull et al., 1967) have revealed that the yield stress in tension and compression are not the same. This is referred to as the tension–compression asymmetry. It is a clear indication of the failure of

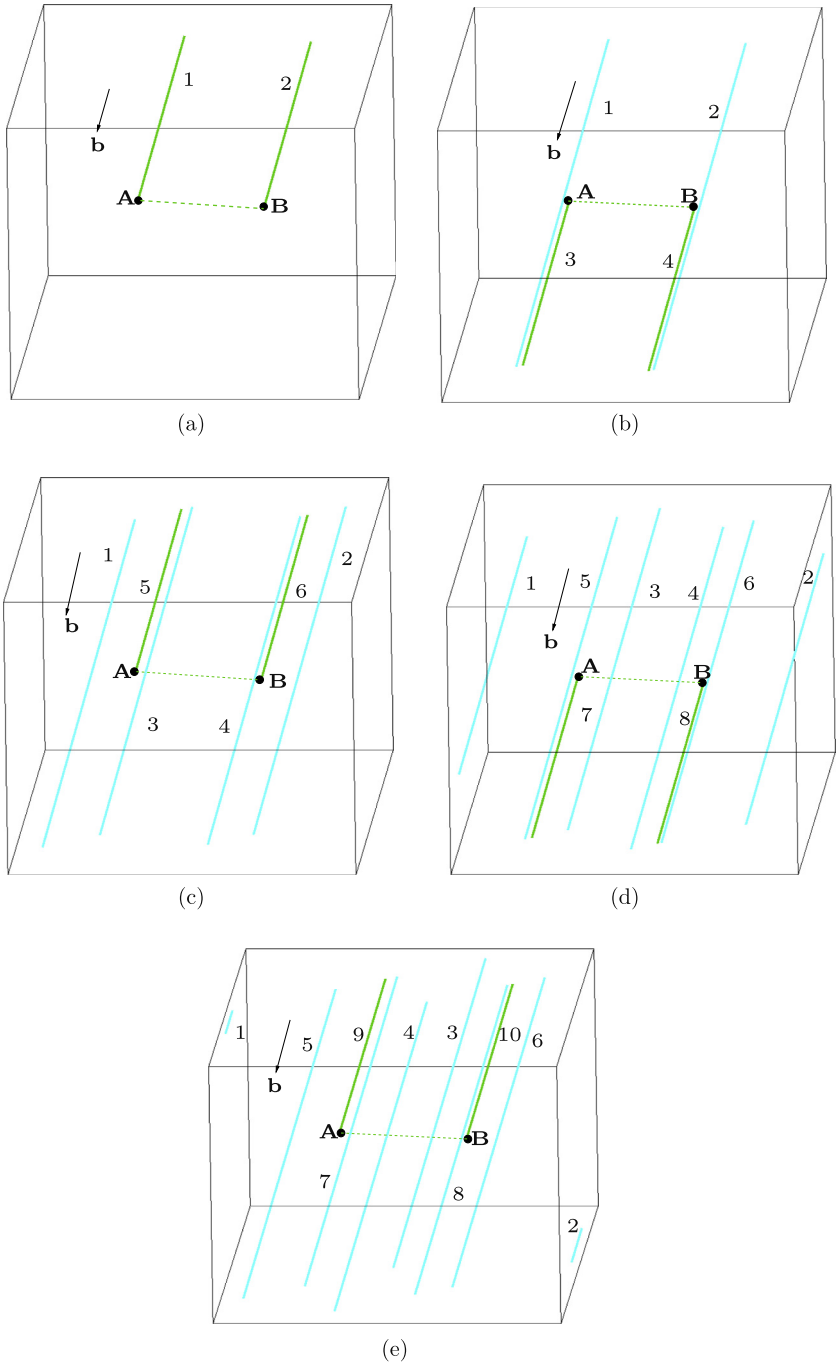

Fig. 10. The figures show the first steps of operation of the Frank–Read source in compression along $[\bar{8}\,20\,27]$with pinning points **A** and **B**. The dislocation lines are colored according to their habit plane. Green color of dislocation means it lies on the $(\bar{1}01)$ plane and cyan indicates the $(\bar{1}10)$ plane. (a) is similar to that in tension but slip occurs in opposite direction because the direction of slip is reversed in compression; (b) the screw dislocations 1 and 2 get activated at their CRSS and move via cross-slip on the $(\bar{1}10)$ plane which has a lower activation enthalpy. The motion of edge dislocations on $(\bar{1}01)$ plane generates further screw dislocation dipoles 3 and 4 respectively; (c) These newly generated spiral sources get activated upon further loading and 3 and 4 move again via cross-slip on parallel $(\bar{1}10)$ planes; (d) the dipole pair 3 and 4 move on parallel planes and hence do not annihilate as in tension; (e) shows that the 3 and 4 are still within and volume and move away from each other on parallel planes with the source being in position similar to sequence (a). (For interpretation of the references in color in this figure legend, the reader is referred to the web version of this article.)

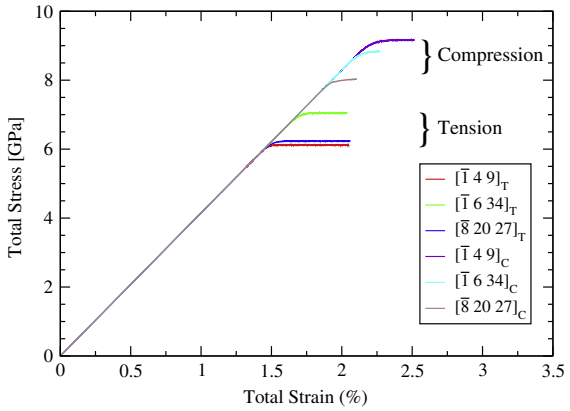

Fig. 11. Normal stress vs strain curves for loading in tension and compression for orientations shown in the legend.

the Schmid law for *bcc* metals. The tension–compression asymmetry generally increases with decreasing temperature (Christian, 1983).

Initially, it was thought to be a consequence of the twinning-antitwinning asymmetry (Argon and Maloof, 1966; Christian, 1983) and therefore a consequence of the sense of shear consistent with tension and compression loadings. This would suggest that the tension–compression asymmetry is an effect intrinsic to *bcc* crystals. Seeger (2002) assumed that this is because slip occurs on {112} planes which are not mirror planes of the *bcc* structure which makes the Peierls potential asymmetric on these planes. He also suggested that additional stress-components other than the resolved stress influence the tension–compression asymmetry. Atomistic studies however reveal that the twinning-antitwinning asymmetry is negligible in tungsten (Gröger et al., 2008a,b). The tension–compression asymmetry, however, is pronounced as shown in Fig. 7. Just as for 0 K (Ito and Vitek, 2001; Gröger et al., 2008a), at finite temperatures too it can be explained as a direct consequence of the effects of the shear stress perpendicular to the slip direction. In terms of model parameters, tensile loading is characterized by $\eta > 0$ ($\sigma > 0$) and compressive loading by $\eta < 0$ ($\sigma < 0$). In Gröger et al. (2008a,b) it was shown that the effect of $\sigma > 0$ is to extend the dislocation core on the primary plane and $\sigma < 0$ to constrict it on this plane and extend it on the other two {110} planes of the same zone. This asymmetry induced by the non-glide component of the stress tensor leads to the lower CRSS in tension than in compression. It decreases with increasing temperature (Christian, 1983; Seeger and Hollang, 2000). Hence, the tension–compression asymmetry is not intrinsic to the lattice but an extrinsically induced effect of the applied loading.

Another characteristic feature of *bcc* metals and often experimentally observed is the dependence of the yield stress on the orientation of the applied loading (Christian, 1983; Seeger and Hollang, 2000; Hull et al., 1967; Argon and Maloof, 1966; Kaun et al., 1968). Again the CRSS in the mesoscopic model extrapolated to 0 K is consistent with the atomistic simulations (Gröger et al., 2008a,b). Note that the CRSS obtained from extrapolation is not exactly equal to the atomistic value because the Peierls barrier is obtained from a fitting function to the atomistic values which leads to some deviation from the exact values. However the order of stresses and the trend in CRSS-dependence on orientation is the same as in the atomistic data. Similar to the tension–compression asymmetry, the orientation dependence also has its origins in the dependence of the Peierls barrier on the non-Schmid components of stress which our model reproduces. This is expected as the model is fitted against the atomistic data at 0 K. As an example, Fig. 7(a) and (c) show the CRSS-T dependencies for different orientations of loading having the same loading ratio η but different MRSSP angles χ and, consequently, different CRSS in tension. In compression, the difference in CRSS is reduced a little because yielding occurs by dislocation motion on the secondary $(\bar{1}10)$ plane for $\chi > 0$ which requires a somewhat lower CRSS.

The orientation dependence of the CRSS reduces considerably with increasing temperature in both tension and compression. At low temperatures, high stresses are applied and the Peierls barrier is strongly deformed. At higher temperatures and lower stresses the Peierls barrier is almost the same for all the glide planes and the energy due to thermal fluctuations plays a greater role. The influence of non-glide stresses therefore vanishes and the dependence of yield stress on orientation disappears.

4.2. Anomalous slip and wavy slip

Slip is defined as anomalous if it occurs on a slip system that does not have the highest resolved shear stress. In this definition, no reference is made to other components of the stress tensor. An anomaly does not exist following the proposed kink pair nucleation energy based model for the screw dislocation mobility in *bcc* metals. The curves in Fig. 8(e)–(g) show that in the low temperature high-stress regime, the activation enthalpy for the cyan region in compression is lowest for slip

on the $(\bar{1}10)$ plane. Hence at lower temperatures for these orientations, the dislocation moves entirely on the $(\bar{1}10)$ plane despite the fact that it has a lower Schmid factor than the $(\bar{1}01)$ plane because it is energetically more favorable.

The question of crystallography of slip in *bcc* metals though investigated extensively in experiments, has not been settled without contradictions. However, a feature common to all *bcc* metals in experiments has been coarse crystallographic slip at low temperatures and non-planar slip at higher temperatures. In all cases the slip direction coincides with a $\langle 111 \rangle$ direction. The interpretations differ with respect to the elementary slip planes on which the kink-pair nucleation occurs. Three common interpretations are found in the literature:

1. The elementary slip planes are of the type $\{110\}$ in the entire temperature range and the MRSSP slip is composed of slip events on $\{110\}$ planes (Chen and Maddin, 1951, 1954).
2. The elementary slip planes are of the type $\{110\}, \{112\}$ and $\{123\}$ (Kaun et al., 1968; Christian, 1983).
3. The elementary slip planes changes from $\{110\}$ at low temperatures to $\{112\}$ at higher temperatures. This interpretation (Seeger, 2002) is based on the argument that at higher temperatures a core transformation of $a/2\langle 111 \rangle$ screw dislocations occurs. This transformation makes it easier for the screw dislocation to glide by elementary steps on the $\{112\}$ planes.

If the $\{112\}$ plane were an elementary slip plane, the dislocations would move exclusively on $\{112\}$ planes and the slip traces would then be coarse under certain loading conditions. However it is experimentally observed that $\{112\}$ slip traces are always wavy (Seeger, 2002; Christian, 1983). However, the approach here is to show that the experimentally observed wavy slip is a natural consequence of the competition of at least two $\{110\}$ slip planes and that it occurs naturally if the non-Schmid stresses are properly taken into consideration.

The average glide plane angle $\overline{\psi}$ displayed in Fig. 8 is computed for different orientations at various temperatures in order to determine the slip trace in tension and compression using Eq. (8). $\overline{\psi}$ is a measure of the amount of deviation of the actual slip plane from the most highly stressed $(\bar{1}01)$ plane. For any orientation in the stereographic triangle shown in Fig. 1, σ is always positive on the MRSSP $(\bar{1}01)$ in tension and vice versa in compression. Since in our model, $\{110\}$ are the elementary slip planes, the contribution of slip from planes other than the primary depends on the effect of loading on these planes. A positive σ means a decrease in energy barrier (because of an extension of the core making it more glissile) on the corresponding most highly stressed $\{110\}$ plane. The effective glide plane then depends on the interplay between σ, χ and η and their effect on the Peierls barrier on all three $\{110\}$ planes. To understand the effect of these components in detail, the twinning and antitwinning cases must be considered separately for tension and compression.

In tension, the simulation results in Fig. 8 clearly show that the slip plane angle $|\overline{\psi}| \leqslant |\chi|$ in the entire temperature range displaying $(\bar{1}01)$ slip at low temperatures and slip on the MRSSP at higher temperatures. For loading in tension along any stress axis in the stereographic triangle considered, the $(\bar{1}01)$ plane has the highest resolved shear stress and the lowest activation enthalpy. Therefore this plane contributes the most to the velocity Eq. (7). To activate a secondary plane, the combined effect of loading and thermal activation must be sufficient to overcome the barrier on the corresponding plane. For low $|\chi|$, the glide stress component on the secondary plane is not sufficient to overcome the Peierls barrier and hence $\overline{\psi} \approx 0$ for a large range of temperatures. With increasing χ, the resolved shear stress on secondary planes increases, leading to a higher probability of kink-pair nucleation and thus plastic slip on the secondary plane increases. Hence in qualitative agreement with experimental observations (Christian, 1983), $\overline{\psi}$ deviates increasingly away from zero towards χ.

For compressive loading corresponding to $\sigma < 0$, the Peierls barrier is always increased on the primary $(\bar{1}01)$ plane compared to the undeformed Peierls barrier due to core constriction on this plane. In general, the dislocation has a higher activation enthalpy on the primary plane irrespective of the orientation of the MRSSP. The $\overline{\psi} - T$ dependencies in Fig. 8 for

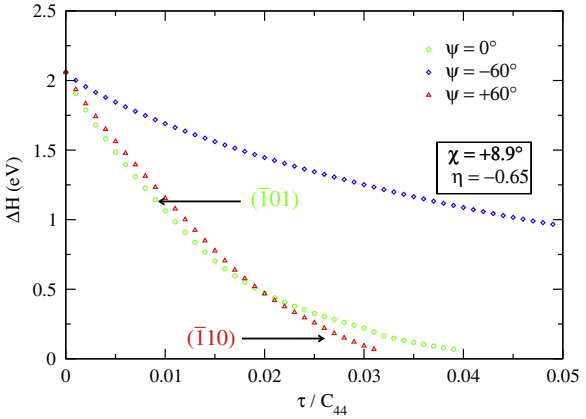

Fig. 12. Stress dependence of activation enthalpy for loading in compression along $[\bar{5}\ 9\ 17]$. The loading parameters are given in the insets.

loading orientations in the magenta region in Fig. 6 are similar to those in tension. Hence, even though the barrier on the primary plane is increased, the activation of the secondary plane is still difficult in antitwinning orientations.

For loading in the cyan region (Fig. 8(e)–(g)), the dislocation motion occurs on the $\psi = +60^\circ$ plane at low temperatures as the activation enthalpy is lowest for this plane. The velocity is therefore almost exclusively governed by the $\psi = 60^\circ$ plane at very low temperatures. With increasing temperatures, the primary plane ($\psi = 0^\circ$) contributes more towards the velocity but the $\psi = 60^\circ$ plane is still the dominant plane.

The competing activity on two planes is illustrated by the following example. The activation enthalpy for motion on the three possible planes for compression loading in the $[\bar{5}\ 9\ 17]$ orientation (c.f. Fig. 8(e)) is shown in Fig. 12 in the entire stress range up to the Peierls stress.

For $\tau/C_{44} > 0.02$ which corresponds to high stresses and low temperatures, the $\Delta H_{\psi=60^\circ}$ on the $\psi = +60^\circ$ plane $(\bar{1}10)$ is smaller than that of the highest resolved $\psi = 0^\circ$ $(\bar{1}01)$ plane. With decreasing stresses (and increasing temperatures), the activation enthalpy on the $\psi = 0^\circ$ $(\bar{1}01)$ plane becomes comparable to the $\psi = 60^\circ$ $(\bar{1}10)$ plane and this plane contributes increasingly to the plastic slip. The $\bar{\psi} - T$ plot computed from these activation enthalpies is shown in Fig. 8(e). The average slip angle changes from $\bar{\psi} = +60^\circ$ at low temperatures and converges towards $\chi = +8.9^\circ$ (so-called irrational slip). This change in activation enthalpy which results in the change of the slip plane from high stress (low temperature) region to low stress (high temperature) for a given χ is a signature of the role of the perpendicular shear stress σ. This is another manifestation of the tension–compression asymmetry in addition to the CRSS dependence on the sense of loading.

The occurence of {110} slip at low temperatures and MRSSP slip with increasing temperatures is consistent with experimental observations in tungsten (Hull et al., 1967; Argon and Maloof, 1966) and several other *bcc* metals (Christian, 1983; Seeger, 2002). This irrational slip often observed in experiments at higher temperatures (Christian, 1983) can be explained entirely in terms of slip on the {110} planes. Recent experimental findings on iron by Caillard (2010) also support this conclusion. It therefore appears not to be necessary to assume that the elementary plane of slip in tungsten and perhaps other *bcc* metals is anything other than the {110} plane.

4.3. Frank–Read sources

The quite different operation of a single FR-source in tension and compression shows the importance of including the non-Schmid behavior. In tension, the approaching dipoles prior to annihilation move faster towards each other. The local stress field and the local MRSSP of the dislocation varies with the distance between the dipoles. For any orientation the local MRSSP is different from the MRSSP due to the macroscopic loading. The degree of variation in the local parameters with respect to the macroscopic value is a function of temperature and dislocation microstructure. Hence in general, the local stress state governing the screw dislocation activation is different from the macroscopic state. Since this may lead to screw dislocations leaving the primary plane of the initial FR-source it means that the initial FR-sources are less important as specific characteristics of the dislocation structure in bcc-metals compared to fcc and may even be indistinguishable from single-armed sources in many cases.

Recently, Wang and Beyerlein (2011) used a different approach to incorporate non-Schmid effects in a DDD model. Their approach utilizes slip on both the {110} and {112} planes in order to capture the orientation dependence and the tension–compression asymmetry in tantalum. Different Peierls stresses for screw and edge dislocations on each of these planes are used along with a modified expression for an "effective Peach–Koehler force" that includes the non-glide components of stresses to capture the non-Schmid effects. The stresses normal to the Burgers vector are used to affect the Peierls stress on the {112} planes only. The Peierls stress values for screw dislocations in their model are taken from experiments. Anomalous slip and the different response of the FR-source in tension and compression as we have shown, cannot be captured with such a description.

4.4. Peierls stress and comparison with experiments

Due to the dependence of the Peierls barrier on the applied loading, it is essential to recall the notion of Peierls stress as deduced from experiments and its comparison with the theoretical value derived from atomistic simulation. The Peierls stress is defined as the critical Schmid stress needed to displace an isolated screw dislocation at 0 K. In contrast, what is referred to as the Peierls stress in experiments is obtained from uniaxial tension and compression tests over a range of temperatures by extrapolating the effective resolved shear stress to 0 K.

As the activation enthalpy, and therefore the Peierls barrier and the Peierls stress depend on the stress tensor $\overline{\boldsymbol{\Sigma}}^{\chi}$, one has to compare the experimental Peierls stress with that obtained from the corresponding loading. We execute this here for the example of the $[\bar{1}49]$ orientation ($\chi = 0^\circ$ and $\eta = 0.51$) for which experimental data are available (Brunner, 2004, 2010). Extrapolation of our data for tensile loading to 0 K gives a value of about 3.6 GPa ($0.022C_{44}$). The value obtained from the atomistic simulations corresponding to $\sigma = 0$ (pure shear parallel to the slip direction) and $\chi = 0^\circ$ is about 4.7 GPa ($0.029C_{44}$) from Gröger et al. (2008a). This means that due to the effect of the shear stress perpendicular to the slip direction a reduction of the Peierls stress by about 25% can be accounted for. As discussed above, the effect of the non-Schmid stresses decreases at higher temperatures. Even at 300 K the reduction of the calculated yield stress in tension as compared to pure shear is of the order of 10%.

It must of course be noted that the obtained value for the Peierls stress from atomistic simulation is still much larger (by about a factor of about 3) than the experimentally deduced Peierls stress even if this correction is made (even for other *bcc* metals see e.g. Proville et al., 2012). Interestingly the discrepancy between the calculated yield stress and the experimental yield stresses remains at this difference of a factor of 3–4 up to room temperature. This discrepancy has been known for some time and several models are discussed to explain it. A lowering of the atomistically determined stress could for example come from the collective glide of dislocations in array (Gröger and Vitek, 2007) or the stress variations in complex dislocation networks. Recently, the influence of zero point vibrations (Proville et al., 2012) has also been proposed as a possible source of this discrepancy. Similarly, the role of interfaces or surfaces for kink-nucleation (Matsui and Kimura, 1973), the influence of vacancies and other crystal defects on kink-pair nucleation, or even the inertia of the dislocation could contribute. It is not our objective here to solve this issue but we want to remark, that recent micropillar compression experiments on tungsten single crystals (Schneider et al., 2011) at room temperature yielded resolved shear stresses of the order of 0.8–1.0 GPa for pillars with diameters above 2 μm and significantly larger resolved shear stresses of the order of 1.5–2.0 GPa for pillars with diameters below 500 nm. Since surface kink nucleation and similar effects should soften the smaller pillars, we take this as indication that the more complex dislocation structures in larger pillars and even more so in macroscopic specimens might aid plastic deformation. Full DDD simulations, based on the implementation presented here, where all short and long-range interactions between dislocations are properly taken into account might shed further light on this discrepancy.

5. Conclusions

This article formulates a multi-scale model for transferring the key atomistic information of screw dislocations to discrete dislocation dynamics models in order to simulate the plastic flow of *bcc* metals in a mesoscale discrete dislocation dynamics framework. The model takes into account the effect of applied loading and incorporates non-glide components of the stress tensor which strongly influence the critical resolved shear stress. The local stress state modifies the Peierls barrier on the three possible glide planes of the screw dislocation and thereby changes the energy barrier for kink-pair nucleation on these planes. The plane with the lowest activation enthalpy then controls the slip of the dislocation.

The model, describing the dislocation activation based on the minimum activation enthalpy of kink-pair nucleation, can account qualitatively very well for the experimentally observed slip on the MRSSP at higher temperatures, the tension–compression asymmetry and the orientation dependence of slip activity. This non-Schmid framework, based on atomistic input, naturally provides a physically based description for the activation of low-Schmid factor planes under compressive loading.

Classically, the {112} and {123} planes have also been considered as elementary slip planes to account for orientation effects. It is shown here that the experimentally observed $\overline{\psi} \rightarrow \chi$ relationship can very well be described by considering {110} as the elementary slip planes only.

Comparing the Peierls stress and the temperature dependence of the flow stress, calculated on single dislocations in our model, between pure shear (usually assumed in atomistic modeling) and tensile loading (usually used in experiments), we demonstrate that the non-Schmid stresses can lower the critical stress by as much as 25%. Nevertheless, the critical stress in agreement with the underlying atomistic data in our model, is still a factor of about 2 to 3 higher than the experimentally observed values even after properly representing the non-Schmid stress contributions of a tensile test. This indicates that dislocation interactions and the complex stress states in dislocation networks may be important to match the experimental situation.

Acknowledgments

The authors acknowldege the financial support of the German Research Foundation (DFG) through Grant DFG Gu-367/30. PG gratefully acknowledges KITP and Materials Department, UC Santa Barbara for partial support of this work through NSF Grants PH11-25915 and DMR-0843934. RG acknowledges support from the Czech Science Foundation, Grant no. P204/10/0255 and from the Academy of Sciences of the Czech Republic, Research Project no. RVO:68081723. This work has also been carried out in part at the Central European Institute of Technology (CEITEC) with research infrastructure supported by the project CZ.1.05/1.1.00/02.0068 financed from the EU structural funds.

References

Argon, A.S., Maloof, S.R., 1966. Plastic deformation of tungsten single crystals at low temperatures. Acta Metall. 14.
Bitzek, E., Gumbsch, P., 2005. Dynamic aspects of dislocation motion:atomistic simulations. Mater. Sci. Eng. A 400–401, 40–44.
Bolton, C.J., Taylor, G., 1972. Anomalous slip in high-purity niobium single crystals deformed at 77 K in tension. Philos. Mag. 26 (6), 1359–1376.
Brunner, D., 2004. Peculiarities of work hardening of high-purity tungsten single crystals below 800 K. Mater. Sci. Eng. A 387–389, 167–170.
Brunner, D., 2010. Temperature dependence of the plastic flow of high-purity tungsten single crystals. Int. J. Mater. Res. 101, 1003–1013.
Brunner, D., Glebovsky, V., 2000. Analysis of flow-stress measurements of high-purity tungsten single crystals. Mater. Lett. 44, 144–152.
Caillard, D., 2010. Kinetics of dislocations in pure Fe. Part I: In situ straining experiments at room temperature. Acta Mater. 58, 3493–3503.
Caillard, D., Martin, J.L., 2003. Thermally Activated Mechanisms in Crystal Plasticity. Pergamon Press.
Chaussidon, J., Robertson, C., Rodney, D., Fivel, M., 2008. Dislocation dynamics simulations of plasticity in Fe laths. Acta Mater. 56, 5466–5476.
Chen, N.K., Maddin, R., 1951. Plasticity of molybdenum single crystals. Trans. A.I.M.E 10, 937–944.
Chen, N.K., Maddin, R., 1954. Slip planes and the energy of dislocations in a body-centered cubic structure. Acta Metall. 2, 49–51.

Christian, J.W., 1983. Some surprising features of the plastic deformation of body-centered cubic metals and alloys. Metall. Trans. A 14, 1237.
Dorn, J.E., Rajnak, S., 1964. Nucleation of kink pairs and the Peierls mechanism of plastic deformation. Trans. A.I.M.E. 230, 1052.
Duesbery, M.S., 1986. The mechanical properties of the dislocation core. Contemp. Phys. 27 (2), 145–168.
Duesbery, M.S., Foxall, R.A., 1969. A detailed study of the deformation of high purity niobium single crystals. Philos. Mag. 20 (166), 719–751.
Gröger, R., Vitek, V., 2005. Breakdown of the schmid law in bcc molybdenum related to the effect of shear stress perpendicular to the slip direction. Mater. Sci. Forum 482, 123–126.
Gröger, R., Vitek, V., 2007. Explanation of the discrepancy between the measured and atomistically calculated yield stresses in body-centered cubic metals. Philos. Mag. Lett. 87, 113.
Gröger, R., Vitek, V., 2012. Constrained nudged elastic band calculations of the Peierls barrier with atomic relaxations. Model. Simul. Mater. Sci. Eng. 20, 035109.
Gröger, R., Bailey, A.G., Vitek, V., 2008a. Multiscale modeling of plastic deformation of molybdenum and tungsten: I. Atomistic studies of the core structure and glide of $1/2\langle 111\rangle$ screw dislocations at 0 K. Acta Mater. 56, 5401–5411.
Gröger, R., Racherla, V., Bassani, J.L., Vitek, V., 2008b. Multiscale modeling of plastic deformation of molybdenum and tungsten: II. Yield criterion for single crystals based on atomistic studies of glide of $1/2\langle 111\rangle$ screw dislocations. Acta Mater. 56, 5412–5425.
Gröger, R., Vitek, V., 2008c. Multiscale modeling of plastic deformation of molybdenum and tungsten: III. Effects of temperature and plastic strain rate. Acta Mater. 56, 5426–5439.
Gumbsch, P., 2003. Brittle fracture and the brittle-to-ductile transition of tungsten. J. Nucl. Mater. 323, 304–312.
Gumbsch, P., Riedle, J., Hartmaier, A., Fischmeister, H.F., 1998. Controlling factors for the brittle-to-ductile transition in tungsten single crystals. Science 282, 1293–1295.
Guyot, P., Dorn, J.E., 1967. Can. J. Phys. 45, 983.
Hartmaier, A., Gumbsch, P., 2005. Thermal activation of crack-tip plasticity: the brittle or ductile response of a stationary crack loaded to failure. Phys. Rev. B 71, 024108.
Hirsch, P.B., 1960. In: Fifth Int. Conf. on Crystallography, Cambridge.
Hirth, J.P., Lothe, J., 1982. Theory of Dislocations. Wiley.
Hull, D., Bacon, D.J., 2001. Introduction to Dislocations, fourth ed. Butterworth–Heinemann, Oxford.
Hull, D., Byron, J.F., Noble, F.W., 1967. Orientation dependence of yield in body-centered cubic metals. Can. J. Phys. 45.
Ito, K., Vitek, V., 2001. Atomistic study of non-Schmid effects in the plastic yielding of bcc metals. Philos. Mag. A 81, 1387–1407.
Jeffcoat, P.J., Mordike, B.L., Rogausch, K.D., 1976. Anomalous slip on Mo-5 at.% Nb and Mo-5 at.% Re alloy single crystals. Philos. Mag. 34, 583–592.
Kaun, L., Luft, A., Richter, J., Schulze, D., 1968. Slip line pattern and active slip systems of tungsten and molybdenum single crystals weakly deformed in tension at room temperature. Phys. Status Solidi 26, 485–499.
Matsui, H., Kimura, H., 1973. A mechanism of the unexpected {110} slip observed in bcc metals deformed at low temperatures. Scr. Metall. 7, 905–914.
Matsui, H., Kimura, H., 1976. Anomalous {110} slip in high-purity molybdenum single crystals its comparison with that in V(A) metals. Mater. Sci. Eng. 24, 247–256.
Mrovec, M., Gröger, R., Nguyen-Manh, D., Pettifor, D.G., Vitek, V., 2004. Bond-order potential for molybdenum: application to dislocation behavior. Phys. Rev. B 69, 094115.
Mrovec, M., Gröger, R., Bailey, A.G., Nguyen-Manh, D., Elsässer, C., Vitek, V., 2007. Bond-order potentials for simulations of extended defects in tungsten. Phys. Rev. B 75, 104119.
Naamane, S., Monnet, G., Devincre, B., 2010. Low temperature deformation in iron studied with dislocation dynamics simulation. Int. J. Plast. 26, 84–92.
Proville, L., Rodney, D., Marinica, M., 2012. Quantum effect on thermally activated glide of dislocations. Nat. Mater. 11, 845–849. http://dx.doi.org/10.1038/nmat3401.
Racherla, V., Bassani, J.L., 2007. Strain burst phenomena in the necking of a sheet that deforms by non-associated plastic flow. Model. Simul. Mater. Sci. Eng. 15 (1), S297–S311.
Riedle, J., Gumbsch, P., Fischmeister, H.F., 1996. Cleavage anisotropy in tungsten single crystals. Phys. Rev. Lett. 76, 3594–3597.
Rodney, D., Proville, L., 2008. Stress dependent Peierls potential: influence of kink-pair nucleation. Phys. Rev. B 79, 094108-1–094110-9.
Schmid, E., Boas, W., 1935. Kristallplastizität. Springer, Berlin.
Schneider, A.S. et al, 2009. Correlation between critical temperature and strength of small-scale bcc pillars. Phys. Rev. Lett. 103, 105501.
Schneider, A.S., Frick, C.P., Clark, B.G., Gruber, P.A., Arzt, E., 2011. Influence of orientation on the size effect in bcc pillars with different critical temperatures. Mater. Sci. Eng. A 528, 1540–1547.
Seeger, A., 1956. On the theory of low-temperature internal friction peak observed in metals. Philos. Mag. 1, 651–662.
Seeger, A., 2002. Peierls barriers, kinks, and flow stress: recent progress. Z. Metall. 93, 651–662.
Seeger, A., Hollang, L., 2000. The flow-stress asymmetry of ultra-pure molybdenum single crystals. Mater. Trans. JIM 41 (1), 141–151.
Tang, M., Kubin, L.P., Canova, G.R., 1998. Dislocation mobility and the mechanical response of b.c.c. single crystals: a mesoscopic approach. Acta Mater. 9, 3221–3235.
Taylor, G.I., Elam, C.F., 1926. The distortion of iron crystals. Proc. R. Soc. A Lond. 112, 337–361.
Vitek, V., 1992. Structure of dislocation cores in metallic materials and its impact on their plastic behavior. Prog. Mater. Sci. 36, 1–27.
Wang, Z.Q., Beyerlein, I.J., 2011. An atomistically-informed dislocation dynamics model for the plastic anisotropy and tension-compression asymmetry of bcc metals. Int. J. Plast. 10, 1471–1484.
Weygand, D., Gumbsch, P., 2005. Study of dislocation reactions and rearrangements under different loading conditions. Mater. Sci. Eng. A 400–401, 158–161.
Weygand, D., Senger, J., Motz, C., Augustin, W., Heuveline, V., Gumbsch, P., 2008. High performance computing in science and engineering '08, Springer-Verlag, pp. 507–523.
Weygand, D., Friedman, L.H., van der Giessen, E., Needleman, A., 2002. Aspects of boundary-value problem solutions with three-dimensional dislocation dynamics. Model. Simul. Mater. Sci. Eng. 10, 437–468.